Turbulent flow properties of large-scale vortex systems

P. S. Bernard[†]

Department of Mechanical Engineering, University of Maryland, College Park, MD 20742

Communicated by Alexandre J. Chorin, University of California, Berkeley, CA, May 19, 2006 (received for review April 1, 2006)

Large-scale computations of dynamically interacting vortex tubes forming filaments are performed with a view toward investigating their relationship to turbulent fluid flow. It is shown that the statistical properties of the tubes are consistent with commonly accepted observations about turbulence such as the Kolmogorov inertial range spectrum and lognormality of the vorticity distribution. A loop-removal algorithm is demonstrated to reduce the nominally exponential growth rate in the number of tubes to linear growth without apparent harm to the underlying physics. In this form, a vortex tube method may become a practical means for simulating high Reynolds number turbulent flows.

gridfree | turbulence | vortex methods

That the dynamical properties of turbulent flow depend on the complex interaction of vortical structures is perhaps its most fundamental property (1, 2). This recognition has motivated efforts toward exploring the statistical mechanics of large systems of vortices (2) as a means toward understanding and explaining why turbulent flow has the characteristics it has. Interest in vortex systems also extends to their use in numerically modeling turbulent flow for applications in engineering and natural systems (3–5). In particular, it has long been thought (6, 7) that representing turbulent flow by freely convecting and interacting vortex elements has the advantage of avoiding the unphysical smoothing that commonly occurs in less than fully resolved grid-based calculations.

The potential advantage of computing turbulence through its vortices has been historically undermined by the dynamical complexity of the phenomenon: the self-determination of a vortex system is an example of an N-body problem and, hence, very expensive computationally. Moreover, the primary physical mechanism of interaction, namely vortex stretching and reorientation, produces convoluted, spatially intermittent vortical structures of intricate detail that tend to require a phenomenally large number of elements for their description through time.

In both of these areas, however, there have been significant advances in recent years that suggest that it is now feasible to perform comprehensive numerical simulations of large vortex systems. In particular, fast methods for solving the N-body problem, such as the fast multipole method of Greengard and Rohklin (8, 9), allow for practical computations involving millions of vortex elements. In an equally important development, Chorin proposed a rationale for hairpin (10), or more generally, loop (2) removal, as a physically consistent means of simplifying the representation of turbulent structures without, possibly, altering the essential physics of the energy cascade. In fact, the vortex stretching process is accompanied by folding that brings energy to small dissipative scales. Direct elimination of folded vortices in the form of loops removes primarily local energy that is likely destined for subsequent dissipation at smaller scales. In this way there is justification for believing that the dynamics of the remaining vortices will not be unduly harmed if vortex loops are removed where and when they form.

The present work considers the computed properties of a turbulent region formed by the short duration pulse of a slotted jet (i.e., a "puff") as simulated by an advanced, parallel implementation of a vortex tube method. It is found that central facets of turbulent flow having to do with energy spectra, correlation and structure functions, the probability density function (pdf) of the vorticity field, and the Hausdorff dimension of the vorticity support are well accounted for by the field of vortex elements. Moreover, loop removal provides enormous benefit in slowing the growth in the computational problem with little or no modification to the underlying physics. It may be concluded from this work that vortex simulations may offer a viable means for probing the nature of high-Reynolds-number turbulent physics as well as forming the basis for practical means for modeling turbulent flow in more general contexts.

Vortex Simulations

Following a standard approach (10, 11), short, straight vortex tubes are used as the primary computational element in representing the flow field. Tubes connected end to end form vortex filaments. Many filaments are present, and their collective positions as defined by the tubes gives an instantaneous representation of the vorticity field of the simulated flow field.

The ith tube out of N total is distinguished according to its end points $\mathbf{x}_i^1$ and $\mathbf{x}_i^2$ and circulation Γ_i and contributes to the velocity field at a point $\mathbf{x}$ according to the Biot–Savart law (5)

$$-\frac{\Gamma_i}{4\pi}\frac{\mathbf{r}_i \times \mathbf{s}_i}{r^3}\,\phi(r/\sigma), \qquad [1]$$

where $\mathbf{r}_i = \mathbf{x}_i - \mathbf{x}$; $\mathbf{x}_i = (\mathbf{x}_i^1 + \mathbf{x}_i^2)/2$; $r = |\mathbf{r}|$, $\mathbf{s}_i = \mathbf{x}_i^2 - \mathbf{x}_i^1$ is the axial vector along the segment; $\phi(r) = 1 - (1 - \frac{3}{2}r^3)e^{-r^3}$ is a high-order smoothing function used for desingularizing the Biot–Savart kernel; and σ is a scaling parameter. A typical value used here is $\sigma = 0.0001$.

Vortex tubes convect via their end points, and if they stretch beyond a maximum distance, say, h, they are subdivided. The circulation of each tube is held constant according to Kelvin's theorem. For computations including loop removal, the filaments are monitored at each time step for locations where vortex tubes contained on the same filament come within close contact of each other. The resultant loop is then excised, and the remaining ends of the filament are rejoined. The algorithm is designed to remove all loops in the flow field at every time step.

The stretching and reorientation of the vortex tubes amounts to a discrete approximation to the convection and vortex stretching/reorientation terms in the vorticity transport equation. For calculations without loop removal, the influence of viscosity is omitted, and the system may be viewed as a numerical solution to the Euler equation. With loop removal present, there is an implied dissipation because local energy is being removed, and it can be imagined, in principle, that the rate of energy loss is a function of parameters such as tube length and radius that could ultimately be tied to a viscosity and Reynolds number. Consid-

Conflict of interest statement: No conflicts declared.

Abbreviation: pdf, probability density function.

[†]E-mail: bernard@umd.edu.

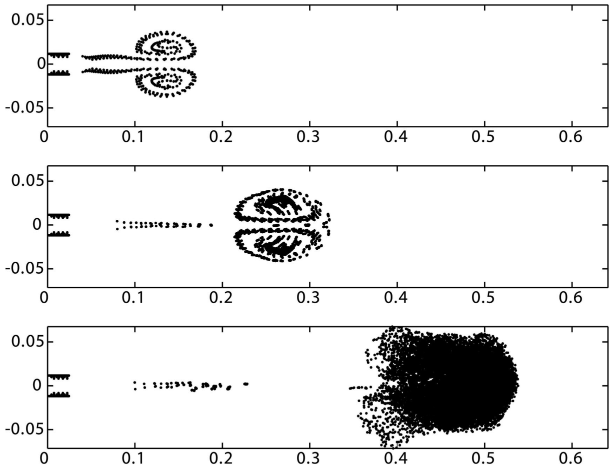

Fig. 1. Side view of vortices in the turbulent puff at times 0.35 (*Top*), 0.71 (*Middle*), and 1.31 (*Bottom*).

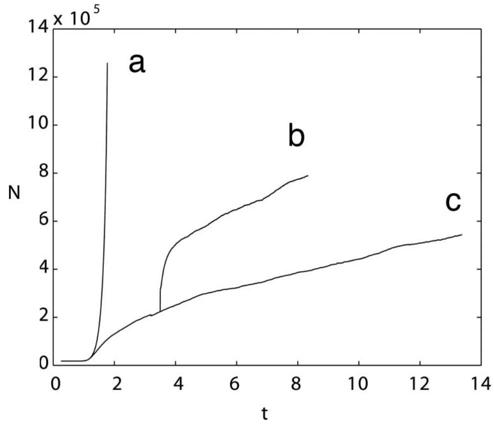

Fig. 3. Number of vortices with time. Line a, no loop removal, $h = 0.0375$; line b, loop removal, $h = 0.025$; line c, loop removal, $h = 0.0375$.

eration of this aspect of loop removal is complicated, however, by the highly transient nature of the turbulent puffs considered here, in which the local energy and volumetric vorticity support change in response to transport processes affecting the size, composition, and shape of the turbulent zone. As a consequence, investigation of the energy field and its dissipation requires further study.

Turbulent Puff

The turbulent puff considered here starts as a jet of short duration that forms into two counterrotating vortices that subsequently succumb to instabilities leading to a turbulent region, as illustrated in side view in Fig. 1. As time proceeds the forward momentum of the vortex system wanes, and the turbulent zone spreads, enlarges, and approaches an isotropic state. A clear view of the dense arrangements of tubes that form in turbulent regions is provided in Fig. 2 showing a round jet computed by the same technique. Here, a lead vortex ring formed at start up has transitioned into a significant collection of turbulent vortex tubes.

The slot in Fig. 1 has unit width ($-0.5 \leq z \leq 0.5$) with periodic extensions imposed to either side to ensure a spanwise periodic velocity field. Image vortex systems with as many as 16 periods to either side of the test section have been considered. The most notable effect of the larger calculations is to lessen or remove spanwise symmetries in the perturbed vortices during the initial transition period that are caused by the imperfect periodicity. After transition, such effects are lost, however, so most computations shown here are done with four images to either side of the test section.

The jet orifice lies between $y = \pm 0.0125$ with x denoting the streamwise direction. The jet has a potential core of unit velocity

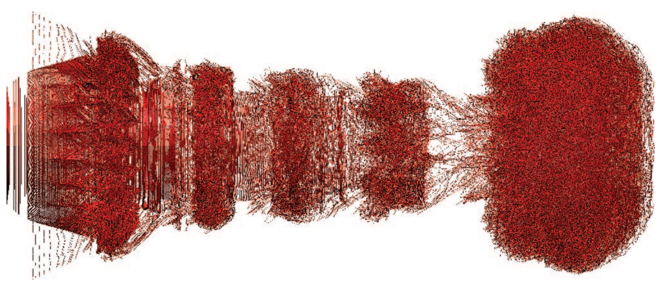

Fig. 2. Turbulent vortices in a round jet.

extending to ± 0.0075 and a linear velocity with constant vorticity imposed in the regions $0.0075 \leq |y| \leq 0.0125$. The latter zones are each subdivided into three equal layers of thickness $d = 0.005/3$ out of which 6 new straight vortex filaments, each composed of 20 tubes of length $h_0 = 0.05$, enter the computational domain at every time step during the formation of the puff. Typically, the turbulent puffs are composed of 6,440 filaments and are formed over a time interval of 0.25. After this time the potential velocity field used in initiating the puff is turned off, and the subsequent behavior of the vortices is exclusively through self-induced motion. It should be noted that because of periodicity, the filaments are, in effect, infinitely long, and so any possible influence there may be from the vorticity $\mathbf{\Omega}$ not satisfying the $\nabla \cdot \mathbf{\Omega} = 0$ identity is removed from the calculations.

Taking U_t and U_b as the velocities at the top and bottom edge of one of the vorticity layers in the nozzle, the material volume of a tube produced during the time interval Δt is $V_0 = h_0 d(U_t + U_b)\Delta t/2$, and its circulation is $\Gamma = \Delta t(U_t^2 - U_b^2)/2$. An initial radius of $r_0 = \sqrt{V_0/\pi/h_0}$ is implied for the tubes. By keeping track of the number of times, say, q_i, a tube subdivides, as in ref. 11, the volume of the ith tube is $V_i = V_0/2^{q_i}$, and its cross-sectional area is $A_i = V_i/s_i$, where $s_i \equiv |\mathbf{s}_i|$ is its length. Assuming constant vorticity over each tube, it follows that the vorticity magnitude at any time is given by $\Omega_i = \Gamma_i/A_i$.

Results

In keeping with the goal of studying the potentially significant effect of loop removal on the physical properties of the vortex systems, calculations are performed both with and without loop removal. Apart from loop removal, the computed turbulent puffs can be expected to be sensitive to the imposed minimum vortex length, h, that controls the range of resolved scales. Beyond this parameter, the only other potentially consequential parameter is the numerical cut-off radius σ, but tests showed that its variation has at best a slight quantitative effect that does not affect the conclusions of this work.

To directly gauge the effect of loop removal two calculations with $h = 0.0375$ were performed that agreed in every way except for the presence or absence of loop removal. A third calculation was initiated from the case with loop removal at time $t = 3.5$, by suddenly reducing h by a factor of 1/3 from 0.0375 to 0.025. The properties of these three runs are representative of what can be expected from the kind of vortex simulations considered here.

The time history of the number of vortices in the three calculations is shown in Fig. 3. Without loop removal, the growth rate is exponentially fast, reaching 1,258,829 tubes at $t = 1.77$. In the last time step of this calculation, 72,802 new vortex tubes

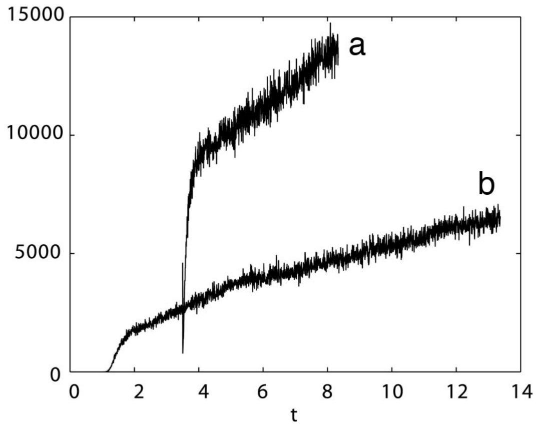

Fig. 4. Number of vortices eliminated at each time step by loop-removal algorithm. Curve a, $h = 0.025$; curve b, $h = 0.0375$.

appear. In contrast, the same run with loop removal has a relatively slow, linear growth in the number of tubes so that it is possible to continue the calculation for a much longer time. Results are shown here up to $t = 13.4$, when there are 555,681 vortices. A similar linear growth rate develops in the case with $h = 0.025$ after an initial transient during which the number of tubes jumps because of the sharper restriction on their length. It may be noted that the linear growth rate is slightly higher for the smaller value of h. This computation was continued to $t = 7.5$ when there were 746,161 vortices.

Fig. 4 shows the number of vortices removed at each time step for the calculations considered in Fig. 3. Evidently, there is quite a bit of variability from time step to time step, although the rate of removal correlates with the total number of vortices. It is clear that as h decreases, the rate of creation of new tubes increases, but so too does the rate of formation of new loops, with the result that the overall tube growth rate remains linear. In the two cases shown in Fig. 4, the cumulative number of tubes eliminated is >10 million, so that the total number that stay in the simulations is actually just a small fraction of those that have made an appearance since the beginning of the puff.

That the number of tubes grows despite the presence of loop removal to a large extent reflects the spread of the turbulence into a larger fluid volume. In fact, the spanwise averaged energy is initially greatest toward the center of the puff but subsequently diminishes and spreads outward as time proceeds. Fixed subvolumes within the central part of the turbulent region, when loop removal is present, appear to have either a constant or slightly declining number of tubes during the course of the simulations. A more complete understanding of the relationship between the number of tubes and the local turbulent statistics requires consideration of the time variation of energy and thus will not be considered here. One last observation is that the process of loop removal also removes volume occupied by vorticity, so that in this case the support of the vorticity field of necessity declines.

The images of turbulent fields in Figs. 1 and 2 are common to flows both with or without loop removal. In contrast, if individual filaments are displayed, such as in Fig. 5, then it is seen that the presence of loop removal causes a significant reduction in the density with which the vortices are packed into a given volume. This disparity, however, does not appear to have great effect on the properties of the turbulent statistics, as now will be considered.

Spectrum. For the purpose of acquiring statistics with which to assess the physicality of the turbulent puffs, velocities are computed on a grid of uniformly spaced points covering the

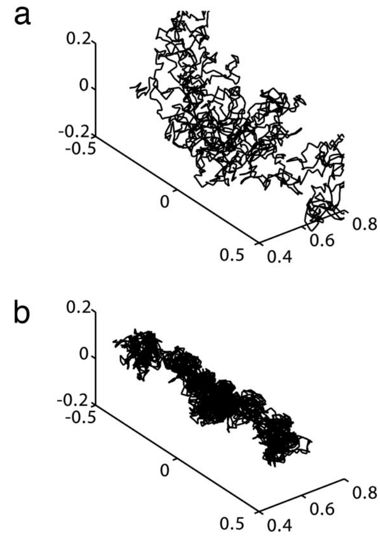

Fig. 5. Vortex filaments in turbulent flow. (*a*) A single filament comprising 1,903 tubes at $t = 13.4$, with loop removal. (*b*) A single filament comprising 3,485 tubes at $t = 1.77$, without loop removal.

spanwise period lying within the region consisting of tubes. Fig. 6 shows the computed velocity components on a typical spanwise cut through a puff, making clear that the data are fully within the turbulent regime.

Spanwise periodicity is particularly convenient for the calculation of one-dimensional velocity spectra using a fast Fourier transform (FFT). Thus, $N + 1$ discrete points are placed in the z direction with velocities at points 1 and $N + 1$ equal to each other. The FFT performed for u, v, w yield the Fourier coefficients $\hat{u}_k$, $\hat{v}_k$, $\hat{w}_k$, respectively, and from these the energy spectrum is computed via

$$E(k) = (\overline{|\hat{u}_k|^2} + \overline{|\hat{v}_k|^2} + \overline{|\hat{w}_k|^2})/2, \qquad [2]$$

where the overbar denotes averaging over many parallel lines through the turbulent zone. For the puff without loop removal, the averaging is done over 841 lines with $N = 1{,}000$ spread uniformly over the domain $0.48 \le x \le 0.62$, $-0.07 \le y \le 0.07$. With loop removal, the later time of the calculation means that the puff has spread further, and accordingly the velocity data are accumulated over the larger region $0.6 \le x \le 0.8$, $-0.15 \le y \le$

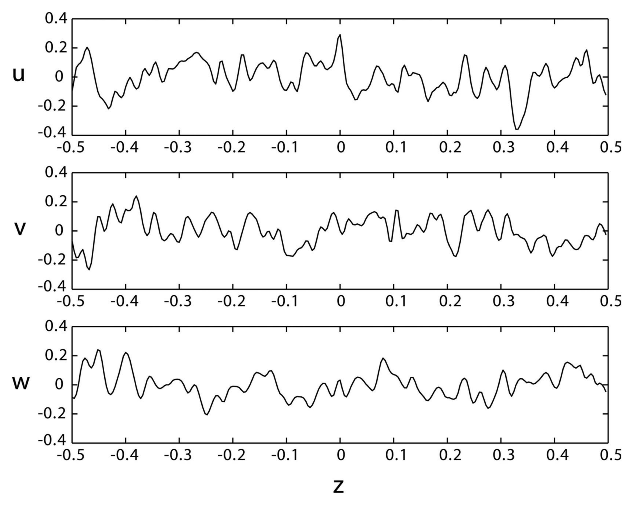

Fig. 6. Velocity traces in the spanwise direction.

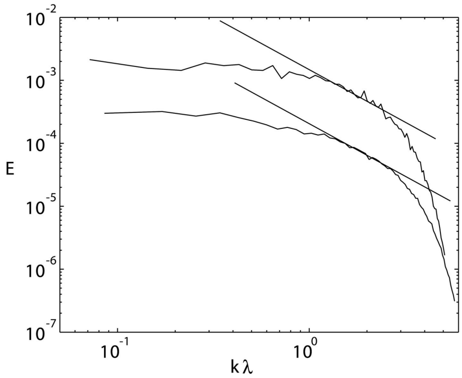

Fig. 7. Energy spectrum. Shown are spectra with no loop removal (upper curve) and loop removal (lower curve). Also shown are lines with $-5/3$ slope.

0.1 covered by a uniform arrangement of 41×51 lines and $N = 250$ points each. In fact, tests showed the energy-containing part of $E(k)$ to be insensitive to N for values >250.

The energy spectra corresponding to puffs with and without loop removal are shown in Fig. 7 where the data with $h = 0.025$ is used for the former. In both cases, the results from the last computed time step is used in the analysis. The larger data set available with loop removal results in somewhat less scatter in the data for this case. The vertical shift of the curves reflects the different average energies of the data sets. Just the largest 3 decades of the energy are plotted. The spectra show characteristics typical of those seen in physical experiments and other simulations (12, 13). Straight lines indicating an exact Kolmogorov $-5/3$ spectrum are included, and it is clear that the data are compatible with this law. Results are plotted in terms of $k\lambda$, where λ is the longitudinal Taylor microscale discussed in the next section.

A closeup view of the $-5/3$ region, which roughly includes wave numbers in the range $1 \leq k\lambda \leq 3$ in both cases, is plotted in Fig. 8. Here, the straight lines are determined by least-squares fits by using the data points indicated with $\times$. The computed slopes without and with loop removal are, respectively, -1.681 and -1.679, values that are slightly higher in magnitude than $-5/3$ and thus perhaps compatible with current views of the role of intermittency (14) in modulating the 5/3 law. More extensive computations will have to be done before a more definitive statement can be made on this point. An important conclusion here is that the inclusion of loop removal appears to have no adverse effect on the energy spectrum or the presence of the Kolmogorov law.

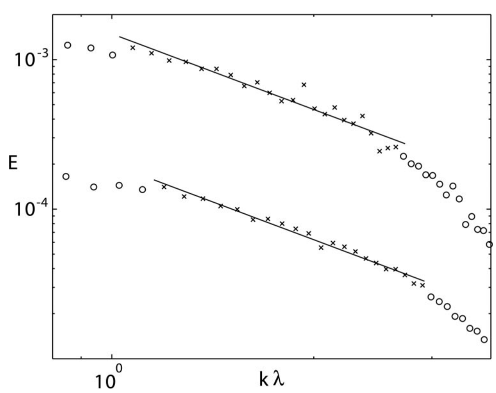

Fig. 8. Detailed view of the inertial range spectrum of Fig. 7. Shown are spectra with no loop removal (upper data) and loop removal (lower data).

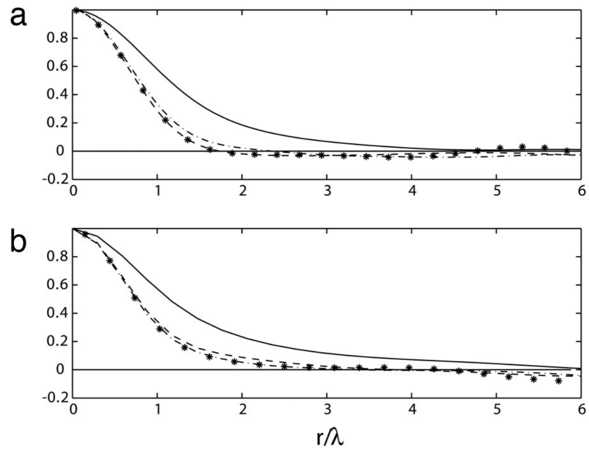

Fig. 9. Correlation functions: f, solid line; g_u, dashed line; g_v, dash-dot line; $f(r) + r/2f'(r)$, $*$. (*a*) Without loop removal. (*b*) With loop removal.

Correlation and Structure Functions. Additional insights into the physicality of the vortex simulations can be had by examining the velocity correlation and structure functions in the light of previous results. By using the same velocity data as previously, the longitudinal correlation function $f(r) = \overline{w(z)w(z+r)}$ and transverse correlation functions $g_u(r) = \overline{u(z)u(z+r)}$ and $g_v(r) = \overline{v(z)v(z+r)}$ were computed in which the separation between points is in the z direction. These functions are shown in Fig. 9 vs. r/λ, where λ is determined from f by fitting a parabola to the data in the vicinity of $r = 0$. It is found that $\lambda = 0.0114$ in the case without loop removal and $\lambda = 0.0136$ with loop removal and $h = 0.025$. For the loop removal case at $t = 13.4$ and $h = 0.0375$, it is found that $\lambda = 0.0142$. These results suggest that either through dissipation or otherwise, loop removal has some effect on raising the minimum resolved scale of the simulations.

The trend in the correlation functions in Fig. 9 is consistent with physical experiments and classical theory as it pertains to isotropic turbulence. In particular, f remains positive, whereas the transverse correlations develop negative regions for sufficiently large separations. The latter two are clearly close to each other in form and distinct from f. If the flow were exactly isotropic then $g_u = g_v$, so by this measure the flow is close to but not exactly isotropic. Another implication of isotropy is the identity $g(r) = f(r) + r/2f'(r)$, where $f' \equiv df/dr$. The right-hand side of this relation is plotted as symbols, and it is seen that this relation well agrees with the transverse correlation function g_v until $r \approx 5\lambda$, where the results begin to show the effects of insufficient averaging. It may be concluded that during the times considered the flow achieves a nearly isotropic state in the y–z plane perpendicular to the direction of the original jet, whereas lingering effects of the startup flow delay the exact appearance of isotropy in the streamwise direction. These conclusions also are supported by the transient behavior of the normal Reynolds stresses in which $\overline{v^2}$ and $\overline{w^2}$ tend to be close in magnitude, whereas $\overline{u^2}$ approaches the other two as time proceeds.

Structure functions representing averages of velocity differences are of interest for what they might reveal about the inertial subrange in the context of physical space. The properties of the simulations considered here limit the amount of averaging available with which to make precise estimates of structure functions, particularly those of high order. Nonetheless, some useful results have emerged, especially from the long time simulation with $h = 0.0375$ where the turbulent zone is most homogeneous. Of note is a computation of the longitudinal structure function $S_p(r) = \overline{|u(x+r) - u(x)|^p}$ for $p = 2, 3, 4$ shown in Fig. 10 that is obtained from averaging over 12,750 lines

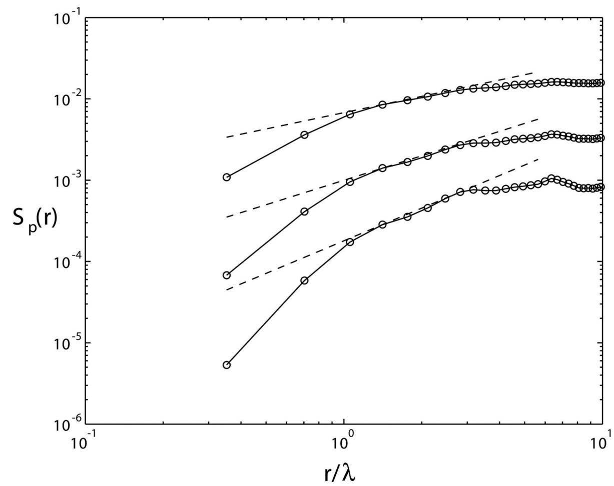

Fig. 10. Structure functions $p = 2, 3, 4$ (top to bottom) for $t = 13.4$, $h = 0.0375$ with loop removal. Straight lines have slopes 2/3, 1, 4/3 (top to bottom).

oriented in the x direction through the puff. Here, log–log plots of the structure functions are shown with straight lines representing power-laws $r^{p/3}$ reflecting the Kolmogorov theory of the inertial range (15). In each case it is seen that the computed results are compatible with theory over an apparent inertial range given approximately by $1 \leq r/\lambda \leq 3$. As in the case of the spectra considered previously, more extensive computations will be needed before nuances associated with shifts in the exponents caused by intermittency can be accurately explored with this technique.

Lognormality. The present computation affords the opportunity to make a more comprehensive examination of the pdf of the vorticity field than has been possible in the past. In particular, theoretical arguments (2, 16) supported by some relatively crude computations (11) have suggested that vorticity satisfies a lognormal distribution, and the goal here is to see whether this hypothesis is supported by the present work. Fig. 11 shows the pdf of $\ln(\Omega)$, where $\Omega \equiv |\mathbf{\Omega}|$, for the computed flows with and without loop removal. The vorticity values used in obtaining the pdf are taken from large sets of tubes contained in a fixed volume of space. Also plotted are Gaussian distributions with mean and variance corresponding to the data.

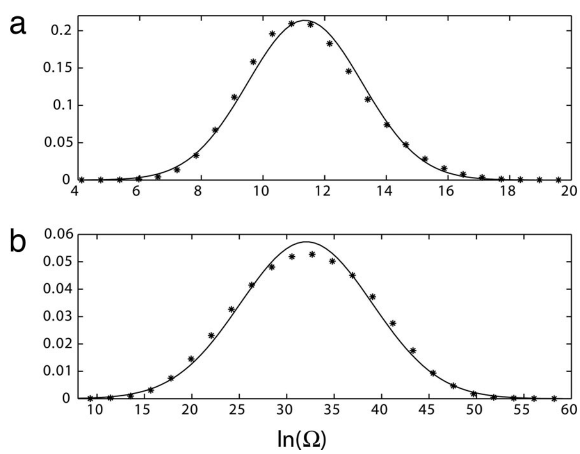

Fig. 11. pdf of $\ln(\Omega)$. *, computed from vortex tubes; solid line, Gaussian determined from vorticity mean and variance. (*a*) Without loop removal. (*b*) With loop removal.

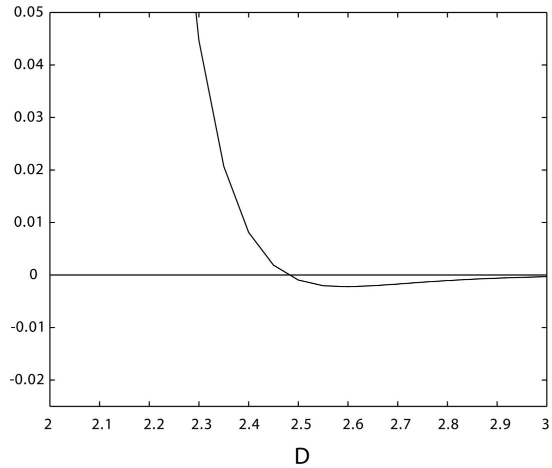

Fig. 12. Slope of $S(D)$ curves vs. D. Zero crossing is at ≈2.483.

In the case without loop removal, there appears to be no doubt that the vorticity obeys a lognormal distribution, because the agreement between the computed and fitted pdfs are excellent. With loop removal, the pdf is close to Gaussian, but the fit is not as exact as in the former case. In particular, there is a slight shortfall in the peak region with a corresponding widening of the distribution. These features are observed for the data taken from both calculations with loop removal and for different times, so it is presumably a real aspect of the loop removal process. If there are any implications of this behavior on the flow physics, they remain to be discovered.

Hausdorff Dimension. It is expected that the end result of vortex stretching in the limit of infinite Reynolds number is to confine the support of the vorticity field to a fractal set. Arguments have been put forward (2) suggesting that the highly resolved vorticity lives on a set of Hausdorff dimension in the neighborhood of 2.5, and this estimate has been supported in computations involving a single turbulent vortex (11). The present computations offer an opportunity to make a more comprehensive assessment of the Hausdorff dimension than previously.

For the present work, the Hausdorff dimension is estimated for the vorticity lying in a fixed central region of space within the turbulent puff. Only the simulation without loop removal is considered because the presence of loop removal prevents the vorticity from evolving toward an ultimate fractal state. Two approaches are considered here. The first is a calculation similar

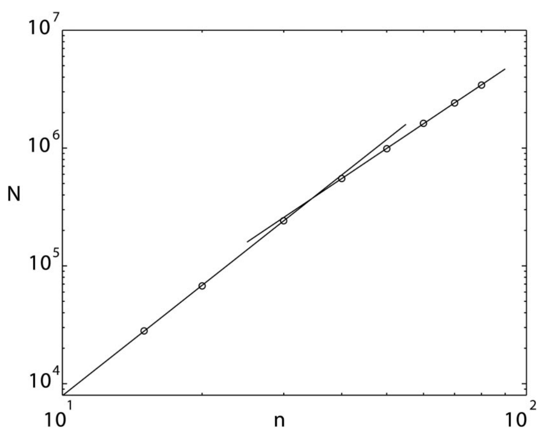

Fig. 13. $N(n)$ vs. n showing shift from slope 3.11 to 2.638 as n increases.

to that in ref. 11 in which the tendency of the radii of the vortex tubes to decrease in time is used as a substitute for covering the vorticity support with a series of diminishing self-similar objects. In particular, the sums $S(D) \equiv \Sigma_i \rho_i^D$, where ρ_i denotes the linear dimension of the ith object used in covering the vorticity, is calculated by means of $S(D) = \Sigma_i s_i r_i^{(D-1)}$, where the sum in this case is over the tubes contained in the fixed region $0.5 \leq x \leq 0.6$, $|y| \leq 0.05$, $|z| \leq 0.5$. The Hausdorff dimension is the value of D for which $S(D)$ remains constant in time. It should be noted that despite the global conservation of the vorticity volume, the volume occupied by vorticity in the subregion used in evaluating $S(D)$ decreases while the number of tubes grows from 272,117 to 629,747 as t ranges from 1.64 to 1.77. The implicit assumption here is that this volume reduction is part of the relaxation toward the final fractal state to which the vorticity is progressing.

The large amount of tubes in the collection volume results in smooth variation in $S(D)$ with time. A precise estimate of the slope of the $S(D)$ curves can be had from least-squares fits, and this slope is plotted in Fig. 12. It is evident that there is a zero crossing to the curve near $D = 2.5$. A linear fit near this point shows that the crossing is at $D = 2.483$, which is thus an estimate of the Hausdorff dimension.

A second scheme for computing D is by means of the box-counting dimension, assuming as it often is, that this method provides a practical substitute for directly computing the Hausdorff dimension of fractal objects (17). The box dimension is obtained by first covering a volume containing the vortices at a fixed time with cubes of various sizes with n denoting the number of cubes lying in one of the coordinate directions. For each n, the number of cubes intersecting the vortex tubes, $N(n)$ is counted, and the estimate of D is taken to be $\lim_{n\to\infty}(\log(\mathrm{N}(\mathrm{n})))/(\log(\mathrm{n}))$. In practical terms, the vortex tubes at a fixed time are not fractal, and D is estimated from a least-squares fit of a straight line to a log–log plot of $N(n)$ vs. n in an appropriate range of n. For small n the slope is expected to be near 3 because a small number of large boxes covers most of the domain. At the other extreme, when n is large, the slope is 3 because many small boxes fit inside the vortex tubes. The box dimension, if it should exist, is the slope of a straight line in a middle range of n. Fig. 13 shows such a calculation for the data at time $t = 1.65$ for which the radii of the tubes is such that the boxes at the upper range of n are just fitting into the tubes. A clear change in slope from 3.11 to 2.638 occurs as determined from least-squares fits. The latter value may be taken as an estimate of the box-counting dimension of the vortex tubes.

The difference between the two estimates of Hausdorff dimension attempted here undoubtedly lies within the uncertainty of the calculations. It is reasonable to conclude that both methods affirm the conjecture that the highly stretched vorticity resides on a fractal set of dimension substantially below 3 and in the neighborhood of 2.5.

Conclusions

The results of this study suggest that beyond their superficial "turbulent" appearance, numerical simulations of vortex tubes forming filaments have characteristics that closely agree with physical experiments and direct numerical simulations of turbulent flow. Among the significant findings is a substantial Kolmogorov inertial range in the energy spectrum that is also revealed appropriately in the structure functions, lognormality of the vorticity field, the approach toward isotropy in the two-point correlation functions, and a Hausdorff dimension for stretched vorticity that is consistent with earlier theory and computation.

An important conclusion of this work is that although loop removal has a dramatic effect in curtailing the explosive growth in the number of vortices, it is not at the expense of the essential physics of the simulation. In fact, apart from some subtle effects on the pdf of $\ln(\Omega)$, the computations with loop removal have similar physics to the undisturbed simulation. Loop removal does affect energy, and finding the nature of this relationship should be a priority for further investigation.

I thank J. Geiger for assistance with the preparation of Fig. 2 and Drs. P. Collins, J. Krispin, and M. Potts for assistance with the development and use of the VorCat, Inc. (Rockville, MD) implementation of the 3D vortex tube method. The computations were performed on the National Science Foundation Terascale Computing System at the Pittsburgh Supercomputing Center.

1. Bernard, P. S. & Wallace, J. M. (2002) *Turbulent Flow: Analysis, Measurement, and Prediction* (Wiley, Hoboken, NJ).
2. Chorin, A. J. (1994) *Vorticity and Turbulence* (Springer, New York).
3. Bernard, P. S., Potts, M. A. & Krispin, J. (2003) in *Proceedings of the 33rd AIAA Fluid Dynamics Conference and Exhibit, Orlando, Florida, June 23–26, 2003* (Am. Inst. of Aeronautics and Astronautics, Reston, VA), Paper 2003-3599.
4. Bernard, P. S., Collins, J. P. & Potts, M. (2005) *SAE Trans. J. Passenger Cars Mech. Syst.*, 612–624.
5. Puckett, E. G. (1993) in *Incompressible Computational Fluid Dynamics: Trends and Advances*, eds. Gunzburger, M. D. & Nicolaides, R. A. (Cambridge Univ. Press, Cambridge, U.K.), pp. 335–407.
6. Chorin, A. J. (1973) *J. Fluid Mech.* **57,** 785–796.
7. Leonard, A. (1975) *Lecture Notes Phys.*, **35,** 245–250.
8. Greengard, L. & Rohklin, V. (1987) *J. Comp. Phys.* **73,** 325–348.
9. Strickland, J. H. & Baty, R. S. (1993) *A Three Dimensional Fast Solver for Arbitrary Vorton Distributions* (Sandia Natl. Lab., Albuquerque, NM), Tech. Rep. SAND93-1641.
10. Chorin, A. J. (1993) *J. Comput. Phys.* **107,** 1–9.
11. Chorin, A. J. (1982) *Commun. Math. Phys.* **83,** 517–535.
12. Gotoh, T., Fukayama, D. & Nakano, T. (2002) *Phys. Fluids* **14,** 1065–1081.
13. Kaneda, Y., Ishihara, T., Yokokawa, M., Itakura, K. & Uno, A. (2003) *Phys. Fluids* **15,** L21–L24.
14. Lesieur, M. (1997) *Turbulence in Fluids* (Kluwer Academic, Dordrecht, The Netherlands).
15. Kolmogorov, A. N. (1941) *Dokl. Akad. Nauk SSSR* **30,** 299–302.
16. Hill, R. J. (1977) *Phys. Fluids* **20,** 2148–2149.
17. Liebovitch, L. S. & Toth, T. (1989) *Phys. Lett. A* **141,** 386–390.